Nanoscale

PAPER

View Article Online
View Journal | View Issue

Raman identification of edge alignment of bilayer graphene down to the nanometer scale

Cite this: *Nanoscale*, 2014, **6**, 7519

Xin Zhang, Qiao-Qiao Li, Wen-Peng Han, Yan Lu, Wei Shi, Jiang-Bin Wu, Arkady S. Mikhaylushkin and Ping-Heng Tan*

The ideal edges of bilayer graphene (BLG) are that the edges of the top and bottom graphene layers (GLs) of BLG are well-aligned. Actually, the alignment distance between the edges of the top and bottom GLs of a real BLG can be as large as the submicrometer scale or as small as zero, which cannot be distinguished using an optical microscope. Here, we present a detailed Raman study on BLG at its edges. If the alignment distance of the top and bottom GLs of BLG is larger than the laser spot, the measured D mode at the edge of the top GL of BLG shows a similar spectral profile to that of disordered BLG. If the alignment distance is smaller than the laser spot, the D mode at a real BLG edge shows three typical spectral profiles similar to that at the edge of SLG, that of the well-aligned edge of BLG, or a combination of both. We show the sensitivity and ability of Raman spectroscopy to acquire the alignment distance between two edges of top and bottom GLs of BLG as small as several nanometers, which is far beyond the diffraction limit of a laser spot. This work opens the possibility to probe the edge alignment of multilayer graphene.

Received 24th January 2014
Accepted 14th April 2014

DOI: 10.1039/c4nr00499j

www.rsc.org/nanoscale

Introduction

Graphene has received much attention due to its unique properties,[1–5] such as near-ballistic transport[6] and high mobility,[7] and its potential applications in nanoelectronics, photonics and optoelectronics.[4,5,8,9] The properties of graphene strongly depend on its edge orientation at different crystallographic directions.[10–14] Edge naturally exists in a graphene sample. The edges also appear in folded or twisted multilayer graphenes[15–18] and when graphene layers are "cut" into nanoribbons[19] and quantum dots.[20] The edge of single-layer graphene (SLG) consists of two different orientations, armchair and zigzag. Only zigzag edges possess localized edge states leading to high local density of states near the Fermi energy, and these states can be spin polarized by Coulombic interactions.[12] In contrast to SLG, the edges of bilayer graphene (BLG) are complicated. Both the top and bottom graphene layers (GLs) of BLG have their own edges, and in an ideal case, the two edges are well-aligned to form an ideal edge of BLG. However, for a real case, there exists an alignment distance h between the edges of the top and bottom GLs of BLG. For example, BLG nanoribbons fabricated by graphene edge lithography show step edges.[21] Multilayer graphenes produced from mechanical exfoliation present at large probability not well-aligned edges.[4] Actually, h can be as large as the submicrometer scale, or as small as several nanometers. $h = 0$ refers to a well-aligned BLG edge. The edge alignment of BLG has profound implications for electron transport through edge channels or for graphene nanoribbons. The localized edge states have recently been observed in measuring the side-gated transport properties of graphene based on graphene-edge field effect transistors (FETs), where the edges of BLG and ten-layer graphene (10LG) are modulated for transporting currents.[22] However, the dependence of conductance on the side gate voltage of these graphene-edge FETs[22] strongly depends on the edge alignments of BLG and 10LG. The edges of two GLs of BLG can mismatch to a large extent where only one edge transports currents.[22] The strips and structural edge roughness had been included to discuss the subgap conductance in gapped BLG theoretically where the effect of edge alignment in real BLG must be considered in the fabricated device.[23] Two possible zigzag step-edges (α and β-steps) on the surface of graphite are modeled and their local density of states are calculated where two different penetration depths have been obtained,[24] which agrees with STM results.[25] Thus, how to probe the edge alignment of BLG, and further of multilayer graphenes, is an open and essential issue.

Raman spectroscopy has historically been an ideal characterization tool within the area of carbon materials,[26–32] especially for studying the defects[33–36] and edges[37–41] by means of the so-called D mode. The amount of defects characterized by the mean crystallite size can be determined by the intensity ratio of D mode to G mode, I_D/I_G.[26,33,34] Edge is a special case of defects in graphene because the translational symmetry has been broken at the edge. For ideal edges, the D mode is zero for

State Key Laboratory of Superlattices and Microstructures, Institute of Semiconductors, Chinese Academy of Sciences, Beijing 100083, China. E-mail: phtan@semi.ac.cn

zigzag edge and large for armchair edge of SLG.[37,39] The study on the Raman spectra of real SLG at the edge shows that I_D/I_G does not always show a significant dependence on edge structures.[39] Although the Raman spectra at the edge of SLG have been well-understood until now,[32,37–41] there are few reports on Raman spectroscopy of the edges of BLG.[42]

Here, we show that Raman spectroscopy is a sensitive and powerful tool to identify the edge alignment of BLG by means of the D and 2D modes. For BLG with well-aligned edges, its D mode at edges exhibits a spectral profile similar to that of the D mode of disordered BLG. If the alignment distance h between the edges of the top and bottom GLs of BLG is smaller than a critical value h_c of ~3.5 nm, the D mode is with a superposed profile from those of disordered SLG and BLG. Once the alignment distance h is larger than h_c, the D peak in the edge region of BLG will exhibit a spectral profile similar to that of disordered SLG. This makes the determination of the alignment distance between the edges of the top and bottom GLs of BLG down to the nanometer scale, far beyond the spatial resolution of a laser spot.

Results and discussion

The Raman spectrum of graphene consists of a set of distinct peaks,[29] similar to the case of graphite whiskers.[43] The G and D modes appear around 1580 and 1350 cm^{-1}, respectively. The G mode corresponds to the E_{2g} phonon at the Brillouin zone center (Γ).[26] The D mode comes from TO phonons around the K point and requires a defect for its activation of the double resonant (DR) Raman process.[29,44] It can only be present in disordered graphene flakes and bulk graphite, or at their edges.[26,33,44] The 2D mode is the second order of the D mode. The 2D mode is always present in pristine and disordered graphene flakes and bulk graphite.[29,33]

In a graphene flake containing both SLG and BLG, there exist three typical edges as indicated by circles in its optical image shown in Fig. 1. The edge of SLG is denoted as SLG_{1E} here. For a graphene layer laid on SLG, there exists a boundary between SLG and BLG. The edge of the top GL of BLG is denoted as BLG_{1E}. The well-aligned edges of BLG are denoted as BLG_{2E}. Raman spectra at the three edges (SLG_{1E}, BLG_{2E}, and BLG_{1E}) are depicted in Fig. 1. Because the D mode at graphene edges, similar to the 2D mode,[45] shows strong dependency on the polarization of the incident laser, all the Raman measurements are obtained with the polarization of the laser beam parallel to the edge orientation by rotating the sample before each measurement. All Raman spectra are normalized by the G mode. The 2D mode at SLG_{1E} is only one Lorentzian peak because Raman scattering for the 2D mode in the visible range is only one process of triple Raman resonance for SLG.[29] However, the D mode at SLG_{1E} shows an asymmetrical profile, which can be fitted by two Lorentzian peaks (D_1 and D_2). The doublet structure of the D mode can be understood by its two different DR processes.[32,46–48] In the DR processes of the D mode, the electrons near K excited by an incident laser can be first scattered by the phonon ω_{D_1} with a vector q_1, or by the edge into the region around K', and then, respectively, scattered back by the edge or the phonon ω_{D_2} with a vector q_2 to recombine with the holes near K. It must be noticed that $q_2 \neq q_1$, and thus $\omega_{D_2} \neq \omega_{D_1}$ due to strong Kohn anomaly for the TO phonon near K.[49] The intensity of the D_1 and D_2 peaks, $I(D_1)$ and $I(D_2)$, is different, $I(D_1) = 4I(D_2)$. Thus, the D_1 peak dominates the D mode.

There are few reports about the detailed spectral profiles of Raman spectra at BLG_{2E}, especially on the D mode.[42] Fig. 1 shows that the 2D mode at BLG_{2E} exhibits an identical spectral profile to that of pristine BLG,[50] being composed of four sub-peaks contributed from different sub-bands of the electronic band structures of BLG.[29] For the D peak, as discussed above, each 2D sub-band corresponds to two sub-peaks of the corresponding D mode where the low-frequency subpeak (D_1) dominates in intensity. As a result, the spectral feature of the D mode at BLG_{2E} is similar to that of the 2D mode as indicated by arrows, but quite different from that at SLG_{1E}. The Raman spectra of ion-implanted SLG (ion-SLG) and BLG (ion-BLG) are also plotted in Fig. 1 for comparison. Ion-implantation induces disorders in SLG and BLG. The disorders activate the D mode in SLG and BLG. Fig. 1 shows that the spectral profiles of the D and 2D modes at SLG_{1E} and BLG_{2E} resemble those of ion-SLG and ion-BLG, respectively. Indeed, edges take the same role in the Raman process of D mode as defects and disorders, which are induced by ion-implantation. For ion-SLG, we found that $I(D_1) = 3I(D_2)$. Because $I(G)$ of ion-BLG is 2 times as much as that of ion-SLG, the efficiency ratio of Raman scattering for the 2D mode of SLG to BLG, η_{2D}, is about 1.3 for the present sample.

The Raman spectrum at BLG_{1E} shows distinctive features to that at BLG_{2E} and SLG_{1E}. The D mode at BLG_{1E} resembles that at BLG_{2E} but with much weaker intensity, while its 2D mode has a spectral feature which is not similar to either BLG_{1E} or SLG_{1E}. To understand the spectral feature at BLG_{1E}, we have drawn an illustration of laser excitation at BLG_{1E} in Fig. 2(a), where the radius of the laser spot is R and the alignment distance h between the top and bottom GLs is larger than R. The laser spot is focused on the boundary of the top GL, *i.e.*, at BLG_{1E}. The Raman spectrum at BLG_{1E} in Fig. 2(a) is from three regions covered by the laser spot: left BLG region, right SLG region and the boundary region of the top GL. The band structures of the BLG and SLG regions are depicted in Fig. 2(b) and (c), respectively. The 2D mode does not need the edges for its activation, so the 2D mode at BLG_{1E} is composed of that of BLG from the left BLG region and that of SLG from the right SLG region. Indeed, the 2D mode at BLG_{1E} in Fig. 1 can be fitted with the line shape of SLG and BLG, as shown by the dashed fitting curves. Because $I(2D)/I(G)$ of SLG is much stronger than that of BLG as discussed before, the 2D mode of SLG dominates the 2D mode at BLG_{1E}. The proportion of the 2D mode between the BLG and SLG components is dependent on the area of BLG and SLG covered by the laser spot at BLG_{1E}. In contrast to the 2D mode, the D mode requires a defect for its activation. We look into the detailed double resonant process of the D mode at BLG_{1E}. The electron in the top GL follows the band structure of BLG, as shown in Fig. 2(b). The laser excitation can create electron–hole pairs in both the top and bottom GLs of BLG. It must be noted that the two GLs are held together by van der

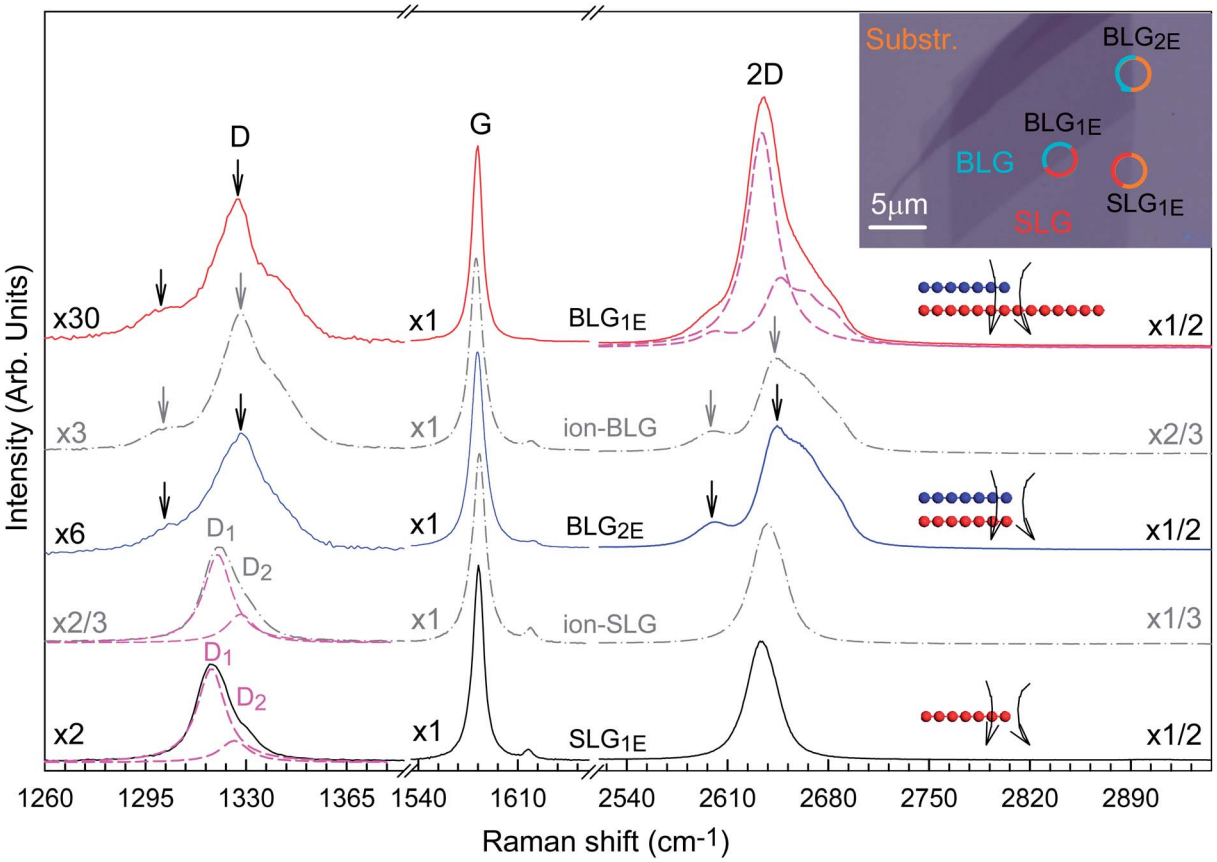

Fig. 1 Raman spectra of three types of edges (SLG_{1E}, BLG_{1E} and BLG_{2E}) in a flake containing both SLG and BLG, which were represented by circles in the inserted optical image. Here, SLG_{1E} denotes the edge of SLG, BLG_{1E} denotes the edge of a graphene layer laid on SLG, and BLG_{2E} denotes well-aligned edges of BLG. Raman spectra of ion-implanted SLG (ion-SLG) and BLG (ion-BLG) are also included for comparison.

Waals interaction with a perpendicular separation much larger than the graphene in-plane lattice so that the photo-excited electrons and holes can only diffuse and be scattered within the same layer. The scattering rate of electrons and holes between adjacent layers can be ignored in comparison with that within the same GL. Within the lifetime of the virtual electron–hole pair in the Raman process,[32] the electrons in the top GL of BLG can be scattered by the D phonon and the edge of the top GL (*i.e.*, BLG_{1E}) and then recombine with the hole in the top GL. The Raman process is a double resonant process with the electronic bands of BLG. So the edge of the top GL can contribute to the observed D mode at the boundary between SLG and BLG and show a corresponding spectral feature of ion-BLG. However, for the photo-excited electrons and holes in the bottom GL at the side of BLG, the Raman process of the D mode is forbidden due to the lack of edge scattering within this layer. Differently, both the top and bottom GLs on the side of BLG contribute to the observed 2D mode. For the well-aligned BLG edge BLG_{2E} shown in Fig. 1, both the edges of the top and bottom GLs can be involved in the resonant Raman process, therefore, the intensity of its D mode is about twice as much as that at BLG_{1E}.

I(G) is proportional to the active area of the graphene layer, which is related by the area exposed by the laser beam, the layer number and edge configuration. The expected I(G) ratio between BLG_{2E} and BLG_{1E} is about 2 : 3. The D mode at the edge of SLG is dependent on the edge orientations. If the edge orientations of the two typical edges are not considered, I(D) is proportional to the active edge length of the graphene layer. The expected I(D) ratio between BLG_{2E} and BLG_{1E} is about 2 : 1. Thus, the expected I(D)/I(G) ratio between BLG_{2E} and BLG_{1E} is about 3 : 1. In Fig. 1, the experimental I(D)/I(G) ratio is 4 : 1. The discrepancy between the estimated and experimental I(D)/I(G) is due to the existence of different zigzag/armchair ratios between the real BLG_{2E} and BLG_{1E} measured here.

Actually, two edges of GLs at BLG_{2E}, as shown in the inset of Fig. 1, may not be aligned perfectly in a real case. It results in a small alignment distance h between edges of two GLs, as illustrated in Fig. 2(a). Once h is smaller than the radius (R) of the laser spot as indicated by the solid circle line, the D mode from SLG_{1E} will appear in the measured spectrum. When $h = 0$, the edges of BLG correspond to well-aligned BLG_{2E}, thus the contribution of SLG_{1E} to the D mode will be zero. To reveal the evolution of the D mode with h from the micrometer scale to zero, the detailed scattering mechanism of the D mode will be considered carefully. Because the D mode is highly localized near the edge of the GL, in principle, its intensity depends on the edge orientation and the edge length. To simplify the discussion, we assume the average edge orientation along the edge of GL in the same sample is similar.[39] Thus, for a large h,

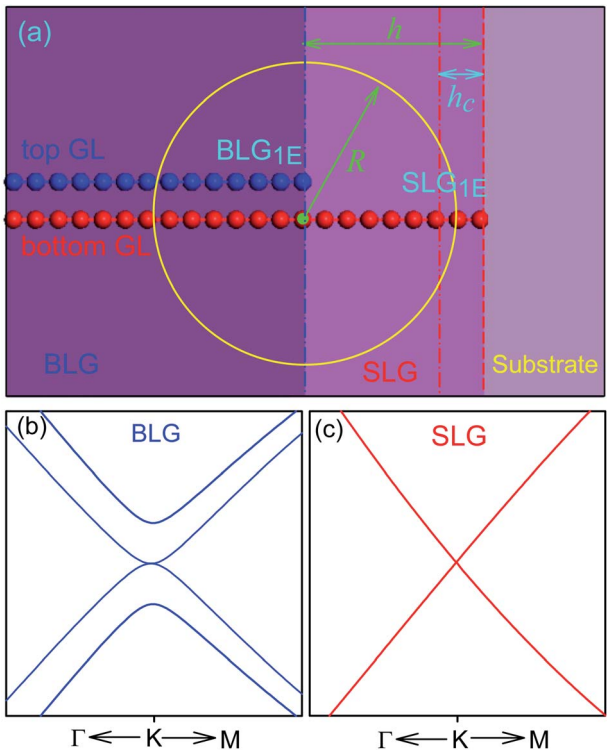

Fig. 2 (a) Schematic illustration of a laser spot focused at the BLG_{1E} of a sample containing two GLs, here R is the radius of the laser spot and h represents the spatial distance between two edges of the top and bottom GLs. (b) Band structure of BLG at the left side of (a). (c) Band structure of SLG extended from the bottom GL of BLG. h_c represents the critical spatial extent at the SLG edge in real space beyond which the electron (or hole) cannot be scattered by the edges.

I(D) is proportional to the length of SLG_{1E} covered by the laser spot. If h is so small that it can be comparable to the lattice constants, the Raman process in real space[51] must be considered to discuss defect-induced Raman modes in the DR Raman process. The photo-excited electron and hole can be treated as quasi-classical particles.[32,39] Their recombination happens when the electron and hole meet each other again in the same region of space size with almost opposite momenta after backscattering events, which puts restrictions on the phonon, defect and incidence angle.[32,37,39] As discussed by Basko's and Ferrari's groups,[38,39] there is a critical spatial extent (h_c) in real space beyond which the electron (or hole) cannot be scattered by the edges. For the D mode, $h_c \sim 3.5$ nm.[32] This means that for a small h, I(D) at SLG_{1E} and BLG_{1E} will be kept constant until h decreases to h_c. If h is larger than h_c and smaller than R, the D mode at the edge of BLG will be composed of that of the edge of SLG (SLG_{1E}) and that of the edge of the top GL of BLG (BLG_{1E}). However, if h is smaller than h_c, the intensity of the D mode at SLG_{1E} will become smaller as h decreases, and finally becomes zero for $h = 0$, *i.e.*, for the well-aligned BLG_{2E}.

Because h_c is as small as about 3.5 nm, the D mode of SLG at not well-aligned edges of BLG ($h > h_c$) will dominate the D band at the edge. Thus, we focus on a real graphene flake to discuss the above intensity evolution of the D mode at the BLG edges. Fig. 3(a) shows the optical image of a BLG flake. At the right lower lateral of BLG, there is a narrow region of SLG. Fig. 3(b) shows the sketch of BLG edges. The AFM images in Fig. 3(c) and (d) indicate that the width of narrow SLG becomes smaller and smaller towards the right upper lateral of BLG, and at last it cannot be distinguished in the AFM images. We have selected some particular spots (sa, sb, sc, sd, se) in proximity to the SLG edge and BLG edge at the right lateral of BLG as marked by circles in Fig. 3(b)–(d). Spots sa and sb correspond to SLG_{1E} and BLG_{1E}, respectively. Spot sc looks like BLG_{2E} from the optical image, however, it contains a narrow piece of SLG with a width of about 100 nm, as revealed from the AFM images, thus is still BLG_{1E}. No SLG region can be recognized by the AFM image at spots sd and se so that the edges here seem to be well-aligned BLG_{2E}.

Fig. 3(e) shows Raman spectra from spots sa–se. Spot sa shows the typical Raman spectrum at SLG_{1E} and that of ion-SLG in Fig. 1, which is with a single Lorentzian peak of the 2D mode and with an asymmetrical spectral profile of the D mode. The Raman spectrum at spot sb resembles that at BLG_{1E} in Fig. 1. However, spot sc shows a typical 2D mode of BLG and a typical D mode of SLG. The 2D mode at spot sc can be actually fitted by the spectral features of SLG and BLG as illustrated by dash-dotted lines, and $I(2D)_{SLG}/I(2D)_{BLG} = 0.16$. The measured I(2D) of SLG and BLG is proportional to the area of SLG and BLG covered by the laser spot at spot sc, respectively. Because h is very small at spot sc, the area ratio of SLG to BLG is about $4h/\pi R$. The measured I(2D) of SLG to BLG is equal to $4h/\pi R^*\eta_{2D} \simeq 1.66h/R$. The width of SLG at spot sc is as small as 48 nm based on the radius of 0.5 μm for the laser spot. For the D mode, the measured I(D) of SLG and BLG is proportional to the edge length of SLG and BLG at spot sc, respectively, if one does not consider the edge orientation. Although h is as small as 48 nm, the edge length of SLG is still comparable to that of BLG_{1E}. From spots sa and sb, the Raman efficiency ratio for the D mode of SLG_{1E} to BLG_{1E}, η_D, is about 2.5. That is why the D mode at spot sc only shows the feature from SLG_{1E} even though its width is as narrow as 48 nm. The Raman spectrum at spot sd shows an identical 2D mode to that of BLG, however, its spectral feature of the D mode is quite different from that at SLG_{1E} and BLG_{1E}. The fitting indicated by dash-dotted lines in Fig. 3(e) shows that the D mode is composed of that of SLG_{1E} and BLG_{1E} with equal peak intensity. As discussed above, the presence of the D mode of SLG_{1E} means that there still exists some partial edge of SLG. However, its intensity is much weaker than the D mode at spots sa and sc. This strongly suggests that h at spot sd is smaller than h_c, but such edge alignment can still be distinguished by the presence of the corresponding D mode. The Raman spectrum at spot se exhibits a typical 2D mode of BLG and an identical spectral feature to the D mode at spot sb, BLG_{1E}. No D and 2D modes related to SLG are observed, indicating that the edge at spot se is close to well-aligned BLG_{2E}. The I(D) at spot se is stronger than that at spot sb because spot se is with contribution from the edges of both the top and bottom GLs.

The above discussion reveals the sensitivity of I(D) and the D-peak profile at the BLG edge on its edge alignment. Similarly, I(D) at well-aligned edges of multi-layer graphene is proportional to the edge length covered by the laser spot, while I(2D) of

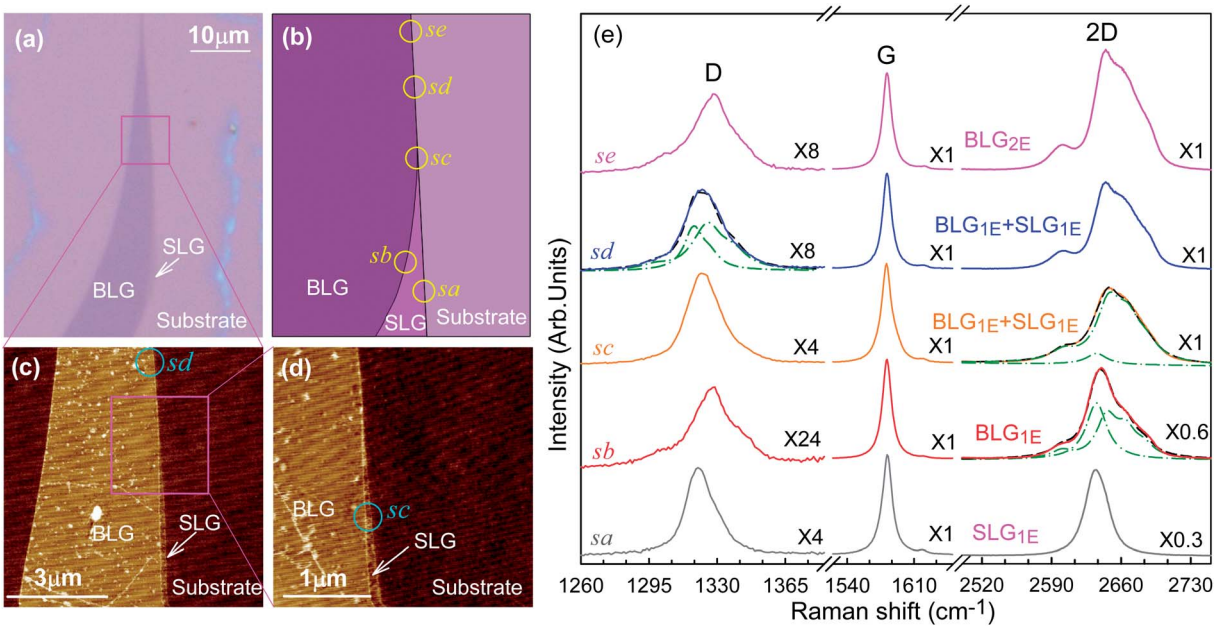

Fig. 3 (a) Optical image of BLG exfoliated on the SiO_2/Si substrate in contact with a small piece of SLG. (b) Sketch map for BLG edges where SLG_{1E} is exaggerated for clarification. (c) AFM image of the sample within the square frame in (a). (d) AFM image of the sample within the square frame in (c). (d) Raman spectra of BLG edges measured at five different spots, sa, sb, sc, sd, and se, as marked in (b–d).

multi-layer graphene is determined by its area covered by the laser spot. Therefore, one can also probe the edge alignment of multi-layer graphene by investigating the D and 2D modes at edges of multi-layer graphene.

Conclusions

In conclusion, we presented the Raman spectra of BLG at its edges. If the alignment distance of the top and bottom GLs of BLG is larger than the laser spot, the measured D mode at the edge of the top GL of BLG shows a similar spectral profile to that of the corresponding ion-BLG, which can be well-understood based on the band structure and DR Raman process. If the alignment distance is smaller than the laser spot, the D mode at real BLG edges shows three typical spectral profiles similar to that at the edge of SLG, that of the well-aligned edge of BLG, or a combination of both. The profile of the 2D mode at the edge is a combination of SLG and BLG whose relative intensity is proportional to the area ratio between SLG and BLG at the edges. It allowed one to get insight into the alignment distance at the edges of BLG from $h \gg h_c$ to $h \ll h_c$. Raman spectroscopy here shows its sensitivity and ability to acquire the edge alignment of BLG down to the nanometer scale, far beyond the diffraction limit of a laser spot and the optical resolution of an optical image. This work benefits further research on fundamental properties on the edges of multi-layer graphenes and edge-based applications.

Methods

Mechanical exfoliation of highly oriented pyrolytic graphite (HOPG) was applied to obtain SLG and BLG samples on a Si substrate with 90 nm SiO_2 on the top.[1,3] No further cleaning or processing was used to maintain the properties of pristine graphene samples. The layer number of each graphene sample was identified by Raman spectroscopy[29,50] and optical contrast.[52–54] Raman spectra were measured in a back-scattering geometry at room temperature with a Jobin-Yvon HR800 Raman system, equipped with a liquid nitrogen cooled charge coupled device, a 100× objective lens (NA = 0.90) and a 600 grooves per mm grating. All Raman spectra were obtained with the polarization of laser beam parallel to the edge by rotating the sample before each measurement. The excitation wavelength is 633 nm of a He–Ne laser. The spectral resolution is ~1.2 cm^{-1}. Atomic force microscopy (AFM) (Dimension edge, Bruker) with non-contact operation mode was used to obtain AFM images with BLG edges. To introduce disorder in graphene flakes, some SLG and BLG samples have been implanted with carbon (^{12}C) ions at ambient temperatures in an LC-4 type system equipped with a C^+ source. The bombardment ion was with a dose of 5×10^{13} C^+ per cm^2 and had a 90 eV kinetic energy.

Acknowledgements

We acknowledge Prof. Yuanbo Zhang and Prof. A. C. Ferrari for useful discussions. We acknowledge support from the special funds for Major State Basic Research of China, contract no. 2009CB929301, the National Natural Science Foundation of China, grants 11225421 and 10934007.

References

1 K. S. Novoselov, A. K. Geim, S. V. Morozov, D. Jiang, Y. Zhang, S. V. Dubonos, I. V. Grigorieva and A. A. Firsov, *Science*, 2004, **306**, 666–669.

2 Y. Zhang, Y. Tan, H. Stormer and P. Kim, *Nature*, 2005, **438**, 201–204.
3 K. S. Novoselov, A. K. Geim, S. V. Morozov, D. Jiang, M. I. Katsnelson, I. V. Grigorieva, S. V. Dubonos and A. A. Firsov, *Nature*, 2005, **438**, 197–200.
4 A. K. Geim and K. S. Novoselov, *Nat. Mater.*, 2007, **6**, 183–191.
5 F. Bonaccorso, Z. Sun, T. Hasan and A. C. Ferrari, *Nat. Photonics*, 2010, **4**, 611–622.
6 X. Du, I. Skachko, A. Barker and E. Y. Andrei, *Nat. Nanotechnol.*, 2008, **3**, 491–495.
7 S. V. Morozov, K. S. Novoselov, M. I. Katsnelson, F. Schedin, D. C. Elias, J. A. Jaszczak and A. K. Geim, *Phys. Rev. Lett.*, 2008, **100**, 016602.
8 F. Torrisi, T. Hasan, W. Wu, Z. Sun, A. Lombardo, T. S. Kulmala, G.-W. Hsieh, S. Jung, F. Bonaccorso, P. J. Paul, D. Chu and A. C. Ferrari, *ACS Nano*, 2012, **6**, 2992–3006.
9 Z. Sun, T. Hasan, F. Torrisi, D. Popa, G. Privitera, F. Wang, F. Bonaccorso, D. M. Basko and A. C. Ferrari, *ACS Nano*, 2010, **4**, 803–810.
10 C. O. Girit, J. C. Meyer, R. Erni, M. D. Rossell, C. Kisielowski, L. Yang, C.-H. Park, M. F. Crommie, M. L. Cohen, S. G. Louie and A. Zettl, *Science*, 2009, **323**, 1705–1708.
11 K. A. Ritter and J. W. Lyding, *Nat. Mater.*, 2009, **8**, 235–242.
12 M. Fujita, K. Wakabayashi, K. Nakada and K. Kusakabe, *J. Phys. Soc. Jpn.*, 1996, **65**, 1920–1923.
13 Y.-W. Son, M. L. Cohen and S. G. Louie, *Phys. Rev. Lett.*, 2006, **97**, 216803.
14 Y.-W. Son, M. L. Cohen and S. G. Louie, *Nature*, 2006, **444**, 347–349.
15 V. Carozo, C. M. Almeida, B. Fragneaud, P. M. Bedê, M. V. O. Moutinho, J. Ribeiro-Soares, N. F. Andrade, A. G. Souza Filho, M. J. S. Matos, B. Wang, M. Terrones, R. B. Capaz, A. Jorio, C. A. Achete and L. G. Cançado, *Phys. Rev. B: Condens. Matter Mater. Phys.*, 2013, **88**, 085401.
16 V. Carozo, C. M. Almeida, E. H. Ferreira, L. G. Cançado, C. A. Achete and A. Jorio, *Nano Lett.*, 2011, **11**, 4527–4534.
17 J. L. Dos Santos, N. Peres and A. C. Neto, *Phys. Rev. Lett.*, 2007, **99**, 256802.
18 K. Kim, S. Coh, L. Z. Tan, W. Regan, J. M. Yuk, E. Chatterjee, M. Crommie, M. L. Cohen, S. G. Louie and A. Zettl, *Phys. Rev. Lett.*, 2012, **108**, 246103.
19 M. Y. Han, B. Özyilmaz, Y. Zhang and P. Kim, *Phys. Rev. Lett.*, 2007, **98**, 206805.
20 P. G. Silvestrov and K. B. Efetov, *Phys. Rev. Lett.*, 2007, **98**, 016802.
21 G. Xie, Z. Shi, R. Yang, D. Liu, W. Yang, M. Cheng, D. Wang, D. Shi and G. Zhang, *Nano Lett.*, 2012, **12**, 4642–4646.
22 H. Goto, E. Uesugi, R. Eguchi, A. Fujiwara and Y. Kubozono, *Nano Lett.*, 2013, **13**, 1126–1130.
23 J. A. Li, I. Martin, M. Buttiker and A. F. Morpurgo, *Nat. Phys.*, 2011, **7**, 38–42.
24 E. V. Castro, N. M. R. Peres and J. M. B. L. dos Santos, *Europhys. Lett.*, 2008, **84**, 17001.
25 Y. Niimi, T. Matsui, H. Kambara, K. Tagami, M. Tsukada and H. Fukuyama, *Phys. Rev. B: Condens. Matter Mater. Phys.*, 2006, **73**, 085421.
26 F. Tuinstra and J. L. Koenig, *J. Chem. Phys.*, 1970, **53**, 1126–1130.
27 R. J. Nemanich and S. A. Solin, *Phys. Rev. B: Condens. Matter Mater. Phys.*, 1979, **20**, 392–401.
28 P. H. Tan, Y. Deng and Q. Zhao, *Phys. Rev. B: Condens. Matter Mater. Phys.*, 1998, **58**, 5435–5439.
29 A. C. Ferrari, J. C. Meyer, V. Scardaci, C. Casiraghi, M. Lazzeri, F. Mauri, S. Piscanec, D. Jiang, K. S. Novoselov, S. Roth and A. K. Geim, *Phys. Rev. Lett.*, 2006, **97**, 187401.
30 S. Reich, C. Thomsen and J. Maultzsch, *Carbon Nanotubes: Basic Concepts and Physical Properties*, Wiley-VCH, 2005.
31 A. Jorio, M. S. Dresselhaus, R. Saito and G. Dresselhaus, *Raman Spectroscopy in Graphene Related Systems*, Wiley-VCH, 2011.
32 A. C. Ferrari and D. M. Basko, *Nat. Nanotechnol.*, 2013, **8**, 235–246.
33 M. M. Lucchese, F. Stavale, E. H. M. Ferreira, C. Vilani, M. V. O. Moutinho, R. B. Capaz, C. A. Achete and A. Jorio, *Carbon*, 2010, **48**, 1592–1597.
34 E. H. Martins Ferreira, M. V. O. Moutinho, F. Stavale, M. M. Lucchese, R. B. Capaz, C. A. Achete and A. Jorio, *Phys. Rev. B: Condens. Matter Mater. Phys.*, 2010, **82**, 125429.
35 L. G. Cancado, A. Jorio, E. H. M. Ferreira, F. Stavale, C. A. Achete, R. B. Capaz, M. V. O. Moutinho, A. Lombardo, T. S. Kulmala and A. C. Ferrari, *Nano Lett.*, 2011, **11**, 3190–3196.
36 Z. H. Ni, T. Yu, Z. Q. Luo, Y. Y. Wang, L. Liu, C. P. Wong, J. Miao, W. Huang and Z. X. Shen, *ACS Nano*, 2009, **3**, 569–574.
37 L. G. Cançado, M. A. Pimenta, B. R. A. Neves, M. S. S. Dantas and A. Jorio, *Phys. Rev. Lett.*, 2004, **93**, 247401.
38 D. M. Basko, *Phys. Rev. B: Condens. Matter Mater. Phys.*, 2009, **79**, 205428.
39 C. Casiraghi, A. Hartschuh, H. Qian, S. Piscanec, C. Georgi, A. Fasoli, K. S. Novoselov, D. M. Basko and A. C. Ferrari, *Nano Lett.*, 2009, **9**, 1433–1441.
40 Y. You, Z. Ni, T. Yu and Z. Shen, *Appl. Phys. Lett.*, 2008, **93**, 163112.
41 D. Zhan, L. Liu, Y. N. Xu, Z. H. Ni, J. X. Yan, C. Zhao and Z. X. Shen, *Sci. Rep.*, 2011, **1**, 12.
42 A. K. Gupta, T. J. Russin, H. R. Gutie'rrez and P. C. Eklund, *ACS Nano*, 2009, **3**, 45–52.
43 P. Tan, C. Hu, J. Dong, W. Shen and B. Zhang, *Phys. Rev. B: Condens. Matter Mater. Phys.*, 2001, **64**, 214301.
44 C. Thomsen and S. Reich, *Phys. Rev. Lett.*, 2000, **85**, 5214–5217.
45 D. Yoon, H. Moon, Y.-W. Son, G. Samsonidze, B. H. Park, J. B. Kim, Y. Lee and H. Cheong, *Nano Lett.*, 2008, **8**, 4270–4274.
46 R. Saito, A. Jorio, A. G. Souza Filho, G. Dresselhaus, M. S. Dresselhaus and M. A. Pimenta, *Phys. Rev. Lett.*, 2001, **88**, 027401.
47 P. H. Tan, L. An, L. Liu, Z. Guo, R. Czerw, D. L. Carroll, P. M. Ajayan, N. Zhang and H. Guo, *Phys. Rev. B: Condens. Matter Mater. Phys.*, 2002, **66**, 245410.
48 P. Venezuela, M. Lazzeri and F. Mauri, *Phys. Rev. B: Condens. Matter Mater. Phys.*, 2011, **84**, 035433.

49 S. Piscanec, M. Lazzeri, F. Mauri, A. C. Ferrari and J. Robertson, *Phys. Rev. Lett.*, 2004, **93**, 185503.
50 W. J. Zhao, P. H. Tan, J. Zhang and J. Liu, *Phys. Rev. B: Condens. Matter Mater. Phys.*, 2010, **82**, 245423.
51 R. Zeyher, *Phys. Rev. B: Solid State*, 1974, **9**, 4439–4447.
52 P. Blake, E. W. Hill, A. H. C. Neto, K. S. Novoselov, D. Jiang, R. Yang, T. J. Booth and A. K. Geim, *Appl. Phys. Lett.*, 2007, **91**, 063124.
53 Z. H. Ni, H. M. Wang, J. Kasim, H. M. Fan, T. Yu, Y. H. Wu, Y. P. Feng and Z. X. Shen, *Nano Lett.*, 2007, **7**, 2758–2763.
54 C. Casiraghi, A. Hartschuh, E. Lidorikis, H. Qian, H. Harutyunyan, T. Gokus, K. S. Novoselov and A. C. Ferrari, *Nano Lett.*, 2007, **7**, 2711–2717.